

Microwave Photonics

UDC 621.391(681.325:535)

Original article

<https://doi.org/10.32603/1993-8985-2020-23-1-52-62>

Statistical Model of a Homodyne Acousto-Optic Spectrum Analyzer

Leonid A. Aronov¹✉, Yurii S. Dobrolensky², Gennadii V. Kulak³

¹Saint Petersburg Electrotechnical University, St Petersburg, Russia

²Space Research Institute of the RAS, Moscow, Russia

³Mozyr State Pedagogical University named after I. P. Shamyakin, Mozyr, Republic of Belarus

✉ aronov.tor@gmail.com

Abstract

Introduction. Interferometric schemes of acousto-optic spectrum analyzers were intended for increasing their dynamic range. The application of these schemes was assumed to provide a twofold increase in the dynamic range expressed in decibels. This article theoretically proves the impossibility of achieving this aim.

Aim. To analyze the noise characteristics of a homodyne acousto-optic spectrum analyzer (HAOSA), as well as to estimate its signal-to-noise ratio and dynamic range.

Materials and methods. A mathematical model describing the HAOSA work was compiled. This model considers the formation of quadrature components for obtaining an amplitude spectrum of an input signal, as well as takes into account the shot and readout noise.

Results. In comparison with an acousto-optical power spectrum analyzer, the application of an interferometric scheme does not provide a twofold increase in the dynamic range. The achieved increase in the dynamic range did not exceed the level of 1.35 dB. Constant illumination led to a significant increase in the self-noise of the spectrum analyzer due to the shot noise, compared to which the thermal noise and the readout noise became insignificant. An expression for estimating the spurious-free dynamic range was obtained, with its value being primarily determined by acousto-optic interaction nonlinearity. Under standard parameters of analyzer blocks, the spurious-free dynamic range is shown to cover a single-signal dynamic range. An expression for estimating the signal-to-noise ratio was derived.

Conclusion. The single-signal dynamic range of a homodyne acousto-optic spectrum analyzer is determined primarily by the photodetector saturation charge. When developing such systems, the question of an optimal ratio of these parameters should be solved, taking into account the light source power, the diffraction efficiency of the acousto-optical modulator and the photodetector saturation charge. The developed statistical HAOSA model provides a more accurate estimation of the dynamic range with an error of 1 dB.

Keywords: homodyne acousto-optic spectrum analyzer, dynamic range, intermodulation distortions, signal-to-noise ratio

For citation: Aronov L. A., Dobrolensky Yu. S., Kulak G. V. Statistic Model of Homodyne Acousto-Optic Spectrum Analyzer. Journal of the Russian Universities. Radioelectronics. 2020, vol. 23, no. 1, pp. 52–62. doi: 10.32603/1993-8985-2020-23-1-52-62

Conflict of interest. Authors declare no conflict of interest.

Submitted 11.07.2019; accepted 15.10.2019; published online 28.02.2020



Статистическая модель гомодинного акустооптического спектроанализатора

Л. А. Аронов¹✉, Ю. С. Доброленский², Г. В. Кулак³

¹Санкт-Петербургский государственный электротехнический университет "ЛЭТИ" им. В. И. Ульянова (Ленина), Санкт-Петербург, Россия

²Институт космических исследований Российской академии наук (ИКИ РАН), Москва, Россия

³Мозырский государственный педагогический университет им. И. П. Шамякина, Мозырь, Республика Беларусь

✉ aronov.tor@gmail.com

Аннотация

Введение. Интерференционные схемы акустооптических спектроанализаторов были разработаны для увеличения динамического диапазона за счет формирования амплитудного спектра исследуемого сигнала вместо спектра мощности. Предполагалось, что это позволит удвоить динамический диапазон, выраженный в децибелах. В настоящей статье показано, что это теоретически невозможно и ожидания, связанные с переходом к интерференционным схемам, завышены.

Цель работы. Анализ шумовых характеристик гомодинного акустооптического спектроанализатора (ГАОСА), оценка отношения сигнал/шум и динамического диапазона на выходе устройства.

Материалы и методы. Представлена математическая модель описания работы ГАОСА с учетом формирования квадратурных компонентов для получения амплитудного спектра входного сигнала. Модель учитывает дробовые шумы и шумы, возникающие при считывании заряда.

Результаты. Показано, что использование интерферометрической схемы не позволяет достичь двукратного выигрыша (при измерении в децибелах) в динамическом диапазоне по сравнению с простой схемой акустооптического спектроанализатора с пространственным интегрированием. Коэффициент увеличения динамического диапазона составляет не более 1.35 дБ. С учетом специфики работы акустооптических устройств получено выражение для оценки динамического диапазона спектроанализатора по интермодуляционным искажениям третьего порядка. Определяющим фактором при этом является нелинейность акустооптического взаимодействия. Показано, что при типовых параметрах узлов устройства динамический диапазон по интермодуляционным искажениям включает в себя односигнальный динамический диапазон. Представлено выражение для оценки отношения сигнал/шум.

Заключение. Односигнальный динамический диапазон ГАОСА определяется в первую очередь уровнем заряда насыщения фотоприемника. При макетировании необходимо решать вопрос оптимального соотношения обоих параметров с учетом мощности источника излучения, эффективности дифракции в акустооптическом модуляторе и заряда насыщения фотоприемника. Представленная статистическая модель ГАОСА с фотоприемником с накоплением дает более точную оценку динамического диапазона с ошибкой в 1 дБ.

Ключевые слова: гомодинный акустооптический спектроанализатор, динамический диапазон, интермодуляционные искажения, отношение сигнал/шум

Для цитирования: Аронов Л. А., Доброленский Ю. С., Кулак Г. В. Статистическая модель гомодинного акустооптического спектроанализатора // Изв. вузов России. Радиоэлектроника. 2020. Т. 23, № 1. С. 52–62. doi: 10.32603/1993-8985-2020-23-1-52-62

Конфликт интересов. Авторы заявляют об отсутствии конфликта интересов.

Статья поступила в редакцию 11.07.2019; принята к публикации после рецензирования 15.10.2019; опубликована онлайн 28.02.2020

Introduction. In comparison with conventional acousto-optic spectrum analyzers based on spatial integration [1, 2], homodyne acousto-optic spectrum analyzers (HAOSA) present interest in terms of having a potentially twofold dynamic range [3–5]. HAOSA are composed of (Fig. 1) a source of monochromatic radiation I , a collimating lens 2, a two-channel acousto-optical modulator (AOM) 3, the channels of which receive the analyzed signal $s(t)$ and the reference signal $r(t)$, a spherical lens 4, and a photodetector (PD) 5.

A spectrum analyzer with an instantaneous PD filter is described in [3], which present little practical interest, since the registration of spatial array distribution requires a line of photodiodes, the output signal of which requires its own processing path. With the advent of matrix PDs with accumulation and numerous cells, a HAOSA scheme with a CCD PD was proposed [6], and a theoretical estimate of the attainable dynamic range was given. At the same time, the authors of [3–5] omitted the fact that, in order to obtain the amplitude spectrum of an input signal $s(t)$, it is necessary to additionally form the quadrature component of the spectrum. Moreover, the empirical values of the dynamic range differed from the theoretical estimate by 4 dB only, thus being far from a twofold increase [6].

Statistical HAOSA model. This article proposes a statistical HAOSA model with a PD with accumulation, which takes into account the formation of quadrature components of the spectrum. On the basis of this model, the estimation of an attainable dynamic range is given.

The HAOSA single-signal dynamic range is defined as

$$DR = 10 \lg \left(\frac{P_{s \max}}{P_{s \min}} \right),$$

where $P_{s \max}$ and $P_{s \min}$ are the maximum and minimum powers of the input harmonic signal, respectively, at which the operability of the device is ensured. The upper limit of the range is determined by two independent phenomena: the nonlinearity of the acousto-optic interaction and the saturation of the PD upon charge accumulation under the influence of radiation. The lower limit is determined by the minimum SNR (signal-to-noise ratio) required by the device.

The main source of HAOSA noise is the PD, which is in turn characterized by two noise types: dependent and independent of the signal level. The latter include thermal noise, which manifests itself as both a dark charge in PD cells and the noise of the electrical circuit forming the current at the PD output.

The presence of photon noise leads to the fact that the charge accumulated by the PD cell under the influence of external radiation is a random variable obeying Poisson statistics. The average number of photoelectrons \bar{n}_e is determined as

$$\bar{n}_e = \bar{n}_{ph} \eta_{PD} T_{acc}, \quad (1)$$

where \bar{n}_{ph} is the average number of photons incident on the cell in 1 s; η_{PD} is the quantum efficiency of the PD; T_{acc} is the accumulation time. The dispersion of the number of photoelectrons is

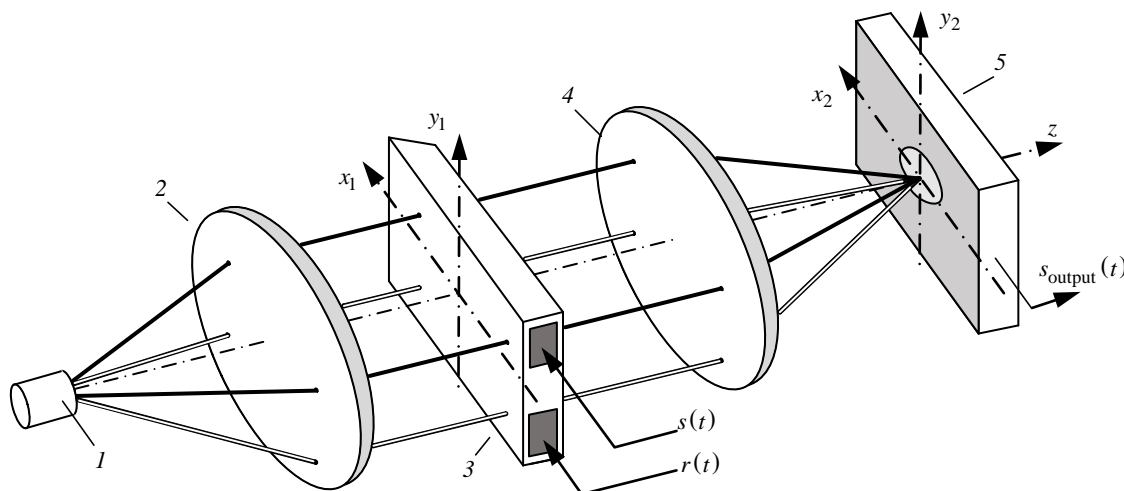


Fig. 1. The Scheme of the Homodyne Acousto-Optic Spectrum Analyzer Based Young Interferometer

$$\sigma_e^2 = \bar{n}_e, \quad (2)$$

which gives $\text{SNR}_e = \bar{n}_e^2 / \sigma_e^2 = \bar{n}_e = \bar{n}_{\text{ph}} \eta_{\text{PD}} T_{\text{acc}}$ at the accumulation stage during T_{acc} .

The charge accumulated by each cell is displayed through the register in time T_{clk} , which gives an average current

$$\bar{i} = (e/T_{\text{clk}}) \bar{n}_e$$

and its dispersion

$$\sigma_i^2 = (e/T_{\text{clk}}) \bar{i}.$$

In this case, the SNR remains unchanged – $\text{SNR}_i = \text{SNR}_e$, while the signal is still subject to Poisson statistics.

The presence of the thermal noise of the electrical circuit increases the dispersion by a dimensionless quantity σ_q^2 . The physical meaning of this quantity is the rms number of electrons of thermal noise over time T_{clk} .

In [7], the noise of the circuit for a field-effect transistor is estimated as

$$\sigma_q \approx \sqrt{B_{\text{PD}}} / 100,$$

where B_{PD} is the working frequency bandwidth of the PD, MHz. Thus, an amplifier with a field-effect transistor has $\sigma_q \approx 500$ at a frequency bandwidth of 100 MHz to 2 GHz.

The resulting SNR at the PD output is:

$$\text{SNR}_{\text{PD}} = \frac{\bar{n}_e^2}{\bar{n}_e + \sigma_q^2}.$$

The charge accumulation in the PD is described by the expression [8]

$$Q(x_2, T_{\text{acc}}) = W_s(x_2, T_{\text{acc}}) + W_r(x_2, T_{\text{acc}}) + 2 \text{Re} \left\{ \int_0^{T_{\text{acc}}} \dot{S}(x_2, t) \dot{R}^*(x_2, t) dt \right\}, \quad (3)$$

where $W_s(x_2, T_{\text{acc}})$ and $W_r(x_2, T_{\text{acc}})$ are the energy spectra of the analyzed and reference signals, respectively, over time T_{acc} ; $\dot{S}(x_2, t)$ and $\dot{R}(x_2, t)$ are the instantaneous spectra of the analyzed and reference signals, respectively; * is a symbol of complex pairing.

Quadrature components can be formed using one of the methods proposed in [9].

In (3), the third term is alternating in sign. For the correct formation of the spectrum of the input signal, the uniform charge on the PD, which corresponds to the energy spectrum of the reference signal $W_r(x_2, T_{\text{acc}})$, should act as a mid-level signal. This means that, in the absence of an input signal, the reference signal should form an average charge in each PD cell $Q_{\text{max}}/2$, where Q_{max} is the maximum charge of the cell. The noise dispersion σ_r^2 , corresponding to such a number of electrons, according to (2) is equal to:

$$\sigma_r^2 = Q_{\text{max}}/2,$$

which, taking into account the noise of the circuit, provides an estimate of the noise variance at the PD output in the absence of the analyzed signal

$$\sigma_{\text{PD0}}^2 = Q_{\text{max}}/2 + \sigma_q^2.$$

This estimate increases in the presence of an input signal that increases the charge accumulated in the cell.

In order to estimate the HAOSA intrinsic noise, let us assume that the average charge of each cell over the PD aperture is $Q_{\text{max}}/2$. This allows the charge distribution in a row to be obtained without distortion according to (3). For modern PDs with accumulation, this value is large enough to approximate the charge distribution in the cell $P(Q_{\text{max}}/2, Q_{\text{max}}/2)$ obeying the Poisson law by the Gaussian distribution $N(Q_{\text{max}}/2, Q_{\text{max}}/2)$ with the required level of accuracy. After reading the charge, the noise dispersion increases due to the noise of the electrical circuit. As a result, the signal at the output of the PD has a distribution $N(Q_{\text{max}}/2, Q_{\text{max}}/2 + \sigma_q^2)$. Following the selection of quadrature components, which corresponds to the elimination of $W_s(x_2, T_{\text{acc}})$ and $W_r(x_2, T_{\text{acc}})$ in (3), 2 signals are obtained. These signals also obey the normal law, but have a zero mathematical expectation and a double dispersion: $N(0, Q_{\text{max}} + 2\sigma_q^2)$. Then, the signal at the HAOSA output calculated as the square root of the sum of squares of quadratures, is determined by a Rayleigh distribution with the dispersion

$$\sigma_{\text{output}0}^2 = (2 - \pi/2)(Q_{\text{max}} + 2\sigma_q^2)$$

and the average

$$m_{\text{output}0} = \sqrt{(\pi/2)(Q_{\text{max}} + 2\sigma_q^2)}.$$

This distribution is not equal to zero and should be taken into account when determining the average distribution in the presence of a signal.

Following similar reasoning, it can be shown that, in the presence of an input signal, the signal at the HAOSA output obeys the Rice distribution:

$$p(s) = \frac{s}{\sigma_N^2} \exp\left(-\frac{s^2 + v^2}{2\sigma_N^2}\right) J_0\left(\frac{sv}{\sigma_N^2}\right),$$

where σ_N^2 is the approximate value of the dispersion of the distributions of the quadrature components; v is the parameter; $J_0(\cdot)$ is a modified Bessel function of the first kind of zero order.

The dispersion of the distributions of quadrature components is estimated as

$$\sigma_N^2 = 2Q_{Wr} + 2Q_{Ws} + 2\sigma_q^2,$$

where Q_{Wr} and Q_{Ws} are the charge components determined by the energies of the reference and analyzed signals, respectively.

The parameter v is equal to:

$$v = Q_s \sqrt{2}, \quad (4)$$

where

$$Q_s(x_2) = 2 \int_0^{T_{\text{acc}}} |\dot{S}(x_2, t)| |\dot{R}(x_2, t)| dt$$

is the value of the useful, informational part of the charge in the cell.

The average value of the signal at the HAOSA output, determined for the Rice distribution:

$$\bar{s}_{\text{output}} = \sqrt{\frac{\pi}{2}} \sigma_N \exp\left(-\frac{v^2}{4\sigma_N^2}\right) \times \left[\left(\frac{v^2}{2\sigma_N^2} + 1\right) I_0\left(\frac{v^2}{4\sigma_N^2}\right) + \frac{v^2}{2\sigma_N^2} J_1\left(\frac{v^2}{4\sigma_N^2}\right) \right],$$

where $J_1(\cdot)$ is the modified Bessel function of the first kind of the first order. The dispersion of the HAOSA output signal is

$$\sigma_{\text{output}}^2 = 2\sigma_N^2 + v^2 - \bar{s}_{\text{output}}^2.$$

Then the SNR at the HAOSA output is

$$\text{SNR}_{\text{output}} = \frac{(\bar{s}_{\text{output}} - m_{\text{output}0})^2}{2\sigma_N^2 + v^2 - \bar{s}_{\text{output}}^2}. \quad (5)$$

It is not possible to solve (5) relative to Q_s ; therefore, the lower boundary of the dynamic range $\text{SNR}_{\text{output}_{\text{min}}}$ can be determined as the limit taking into account the smallness of v :

$$\begin{aligned} \text{SNR}_{\text{output}_{\text{min}}} &= \lim_{\frac{v^2}{2\sigma_N^2} \rightarrow 0} \frac{(\bar{s}_{\text{output}} - m_{\text{output}0})^2}{2\sigma_N^2 + v^2 - \bar{s}_{\text{output}}^2} = \\ &= \frac{(\pi/2) [v^2 / (2\sigma_N^2)]^2}{2\sigma_N^2 - (\pi/2)\sigma_N^2 + v^2}, \end{aligned}$$

moreover,

$$\lim_{\frac{v^2}{2\sigma_N^2} \rightarrow 0} \sigma_N^2 = (Q_{\text{max}} + 2\sigma_q^2).$$

Following mathematical transformations, a square equation relative to v^2 is obtained, the positive root of which and (4) will give an estimate of the lower boundary of the dynamic range in the form of

$$\begin{aligned} Q_{s_{\text{min}}} &= \left(\frac{Q_{\text{max}} + 2\sigma_q^2}{\pi} \left\{ 2\text{SNR}_{\text{output}_{\text{min}}} + \right. \right. \\ &\left. \left. + \left[4\text{SNR}_{\text{output}_{\text{min}}}^2 + 2\pi\text{SNR}_{\text{output}_{\text{min}}} \left(2 - \frac{\pi}{2} \right) \right]^{0.5} \right\} \right)^{0.5}. \quad (6) \end{aligned}$$

This value determines the relative level of the HAOSA output signal, at which the specified minimum SNR is achieved: $\text{SNR}_{\text{output}_{\text{min}}}$.

The upper boundary of the dynamic range, determined by the capabilities of the PD, corresponds to $Q_{s_{\text{max}}}$, at which the charge of the PD cell reaches the maximum allowed value Q_{max} . Let us give an estimate of $Q_{s_{\text{max}}}$ provided that the charge accumulation of the cell is described by (3). The spatial carrier will not be taken into account, assuming that, at some point, the third term can reach a positive maximum:

$$Q_{s_{\text{max}}} = Q_{\text{max}} (\sqrt{2} - 1). \quad (7)$$

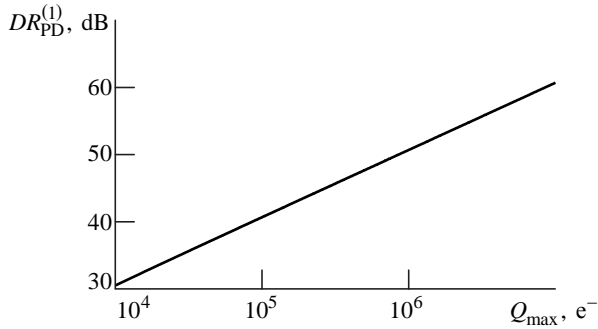


Fig. 2. 1dB Compression Dynamic Range

Single-signal dynamic range. The ratio of (7) to (6) defines a single-signal dynamic range limited by the capabilities of the PD:

$$DR_{PD}^{(1)} = 20 \log \left\{ \frac{Q_{\max} (\sqrt{2} - 1)}{Q_{s_{\min}}} \right\}. \quad (8)$$

Let us evaluate $DR_{PD}^{(1)}$ for the standard PD parameters: saturation charge $Q_{\max} = 10^5 e^-$, the noise of electric circuits $\sigma_q^2 = 2 \cdot 10^2$. Under $SNR_{\text{output}_{\min}} = 1$, the single-signal dynamic range of HAOSA, limited by the capabilities of the PD, will be 40 dB. This means an increase in the dynamic range of about 1.35 times instead of the expected 2 times. The main limiter for $DR_{PD}^{(1)}$ is the saturation charge of the PD, which determines both the upper and lower limits of the range. The dependence of $DR_{PD}^{(1)}$ on Q_{\max} is presented in Fig. 2.

Signal-to-noise ratio. Calculations according to (5) give an estimate of the SNR of the HAOSA output signal for various values of Q_s (Fig. 3).

To assess the radiation intensity I , forming in time T_{acc} the average charge \bar{Q} in a cell with an ar-

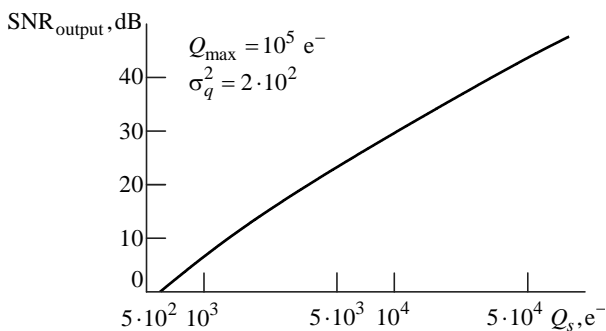


Fig. 3. Signal-to-Noise Ratio Versus Signal Component Charge Level

ea S_{cell} , the relation (1) can be used to obtain:

$$I = \frac{\bar{Q} \hbar \omega}{e S_{\text{cell}} \eta_{PD} T_{\text{acc}}} = \frac{\bar{n}_e \hbar \omega}{S_{\text{cell}} \eta_{PD} T_{\text{acc}}},$$

where \hbar is Planck's constant; ω is the frequency of the light wave; e is the electron charge.

Then the radiation intensity in the reference channel, which will provide a charge $Q_{\max}/2$ in each cell, should be

$$I_R = \frac{Q_{\max} \hbar \omega}{2e S_{\text{cell}} \eta_{AG} T_{\text{acc}}}.$$

To form a charge Q_s , containing information about the spectrum of the input signal, it is necessary to ensure the intensity in the signal channel

$$I_S = \frac{2Q_s^2 \hbar \omega}{Q_{\max} e S_{\text{cell}} \eta_{PD} T_{\text{acc}}}.$$

The radiation powers necessary for the formation of the required charge in n_{cell} cells of the PD in the reference and signal channels will be:

$$P_r = n_{\text{cell}_r} \frac{Q_{\max} \hbar \omega}{2e \eta_{PD} T_{\text{acc}}}; \quad P_s = n_{\text{cell}_s} \frac{2Q_s^2 \hbar \omega}{Q_{\max} e \eta_{PD} T_{\text{acc}}}.$$

The number of cells in the signal channel n_{acc_s} when determining a single-signal dynamic range must correspond to one spectral resolution element, while the number of cells in the reference channel n_{acc_r} must correspond to the total number $N_{\text{res.el.}}$ of resolution elements in the spectrum. Provided that three lines of the PD aperture should be read and selecting 3 cells on the main PD lobe, let us take $n_{\text{cell}_s} = 9$ and $n_{\text{cell}_r} = 9N_{\text{res.el.}}$.

The light intensity in the first diffraction order $I^{\pm 1}$ in the Bragg mode is related to the intensity I_{inc} of the radiation that is incident on the AOM by the relation [10]

$$I^{\pm 1} = \sin^2 \left(\frac{\pi}{\lambda \cos \theta_B} \sqrt{\frac{M_2 P_{\text{sw}} l}{2b}} \right) I_n = \eta_B (P_{\text{sw}}) I_n. \quad (9)$$

where λ is the wavelength of light; θ_B is the Bragg angle for the reference channel AOM; M_2 is the diffraction quality of the AOM material; P_{sw} is the sound wave power; l is the length of the acousto-

optical interaction; b is the width of the AOM piezoelectric transducer; η_B is the diffraction efficiency in the Bragg mode.

Multiplying the left and right sides of (9) by the longitudinal sectional area of the acoustic beam, let us turn to the calculation of powers and determine the radiation level required for exposure to the reference and signal channels:

$$P_{inc_r} = \frac{P_r}{\eta_{B_r}(P_{sw_r})} = n_{cell_r} \frac{Q_{max} \hbar \omega}{2e \eta_{PD} T_{acc} \eta_{B_r}(P_{sw_r})};$$

$$P_{inc_s} = \frac{P_s}{\eta_{B_s}(P_{sw_s})} = n_{cell_s} \frac{2Q_s^2 \hbar \omega}{Q_{max} e \eta_{PD} T_{acc} \eta_{B_s}(P_{sw_s})}, \quad (10)$$

where $\eta_{B_r}(P_{sw_r})$ and $\eta_{B_s}(P_{sw_s})$ are the dependences of the diffraction efficiency in the Bragg mode on the sound power in the reference and signal channels of the AOM, respectively. Thus, the required charge level can be ensured by both P_{sw} , i.e. the level of the AOM input signal, and the laser radiation power.

Nonlinearity of acousto-optical interaction.

For further consideration, let us represent (9) in the form of

$$I^{\pm 1} = \sin^2(C_{AOM} \sqrt{P_{sw}}) I_{inc},$$

where C_{AOM} is a constant. AOM can be characterized by the diffraction efficiency $\eta_{B_{eff}}$ per 1 W of acoustic power, which ranges from fractions to tens of percent. Then, for the constant,

$$C_{AOM} = \arcsin(\sqrt{\eta_{B_{eff}}}).$$

Let us consider the dependence $\eta_B(P_{sw})$ at $\eta_{B_{ef}} = 0.5\%$ (Fig. 4). A 1-dB deviation of the de-

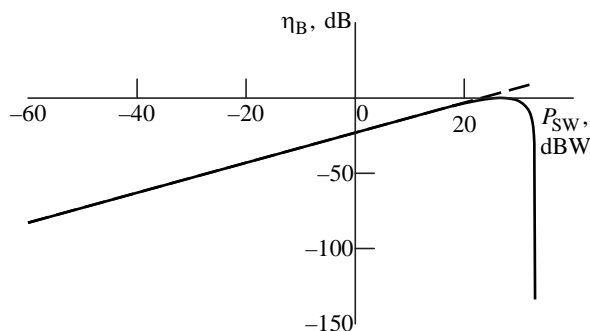


Fig. 4. Bragg Diffraction Efficiency Versus Acoustic Signal Power

pendence on the linear law (dashed line) is observed at a sound power of 21 dB/W, which can be considered the upper limit for the input signal level when considering the nonlinearity of the acousto-optical interaction. The diffraction efficiency $\eta_{B_{max}}$ in this case is more than 60%. Calculations show that a 10-fold decrease in $\eta_{B_{ef}}$ raises the upper bound by about 9 dB.

Let us estimate P_{inc_r} for the following parameters, which can be considered standard:

- diffraction efficiency per 1 W of sound power $\eta_{B_{ef}} = 0.5\%$;
- power of the acoustic signal $P_{sw_r} = 1$ W;
- the saturation charge of the PD $Q_{max} = 10^5 e^-$ [11, 12];
- quantum efficiency of the PD $\eta_{PD} = 0.5$ [11, 12];
- time of charge accumulation at the PD $T_{acc} = 100 \mu s$ [11, 12];
- the number of cells of the PD in three rows $n_{cell_r} = 9000$.

Calculations show that the charge $Q_{max}/2$ in 9000 cells can be provided by the power $P_{inc_r} \cong 0.55$ mW. This value is lower than the upper linearity limit of acousto-optic interaction by more than 20 dB. Assuming for simplicity $P_{inc_r} = P_{inc_s}$, the sound power in the signal channel can be determined, at which the PD is saturated, i.e., the upper limit $DR_{PD}^{(1)}$ is reached. For a harmonic signal, this value will be $P_{sw_s} \cong 0.69$ mW. In this case, the efficiency of diffraction in the signal channel comprises $\eta_{B_s} \cong 0.0034\%$.

When assessing the laser radiation power P_{las} , it is necessary to take into account the losses associated with the inefficiency of beam focusing, light scattering in the optical path, etc. Assuming the laser utilization factor equal to 1%, $P_{las} \approx 100$ mW. In this mode, the single-signal dynamic range of the HAOSA is determined exclusively by the capabilities of the PD and is calculated according to (8).

Two-signal dynamic range. Let us evaluate the level of intermodulation distortions of the third order. In a HAOSA, the nonlinearity determining the two-signal dynamic range $DR_{HAOSA}^{(2)}$ is associated with

acousto-optical interaction. Let us express $\eta_{B_s}(P_{sw_s})$ from (10):

$$\eta_{B_s}(P_{sw_s}) = \frac{2Q_s^2 \hbar \omega n_{cell_s}}{Q_{max} e \eta_{PD} T_{acc} P_{inc_s}} \quad (11)$$

and use the fact that $\eta_{B_s}(P_{sw_s}) = \sin^2(C_{AOM} \sqrt{P_{sw_s}})$. Extracting the root from the right and left sides of (11),

$$\sin(C_{AOM} \sqrt{P_{sw_s}}) = Q_s \sqrt{\frac{2 \hbar \omega n_{cell_s}}{Q_{max} e \eta_{PD} T_{acc} P_{inc_s}}}$$

Let us expand the sine function on the left side of the equality in a Taylor series, leaving the first 2 terms in the record:

$$\begin{aligned} C_{AOM} \sqrt{P_{sw_s}} - \frac{(C_{AOM} \sqrt{P_{sw_s}})^3}{6} + \dots = \\ = Q_s \sqrt{\frac{2 \hbar \omega n_{cell_s}}{Q_{max} e \eta_{PD} T_{acc} P_{inc_s}}} \end{aligned} \quad (12)$$

In this expression, the first term on the left determines the linear component of the signal, and the second is the third-order intermodulation products. To determine the lower boundary of the two-signal dynamic range in (12), it is necessary to leave the first term on the left and substitute Q_s on the right with $Q_{s\min}$, which is defined according to (6). As a result of mathematical transformations, an expression for the input signal level $P_{sw_s\min}$ corresponding to the lower boundary of the dynamic range can be obtained:

$$P_{sw_s\min} = \frac{Q_{s\min}^2 2 \hbar \omega n_{cell_s}}{Q_{max} e \eta_{PD} T_{acc} P_{inc_s} C_{AOM}^2}$$

In order to determine the upper boundary of the two-signal dynamic range in (12), it is necessary to leave the second term on the left without taking into account the sign, and to substitute Q_s on the right with $Q_{s\min}$. After mathematical transformations, an expression for the input signal level $P_{sw_s\max}$ corresponding to the upper boundary of the two-signal dynamic range is obtained as:

$$P_{sw_s\max} = \frac{\sqrt[3]{\frac{72 Q_{s\min}^2 \hbar \omega n_{cell_s}}{Q_{max} e \eta_{PD} T_{acc} P_{inc_s}}}}{C_{AOM}^2}$$

The relation $P_{sw_s\max}$ to $P_{sw_s\min}$ defines a two-signal dynamic range. On a logarithmic scale, this quantity is defined as

$$DR_{HAOSA}^{(2)} = \frac{10}{3} \log 9 + \frac{20}{3} \log \frac{Q_{max} e \eta_{PD} T_{acc} P_{inc_s}}{Q_{s\min}^2 \hbar \omega n_{cell_s}}$$

Let us estimate $DR_{HAOSA}^{(2)}$ for the following parameters:

– radiation power incident on the AOM signal channel $P_{inc_s} = 0.55$ mW;

– saturation charge of the PD $Q_{max} = 10^5$ e⁻;

– the noise parameter of the PD scheme $\sigma_q^2 = 2 \cdot 10^2$, which gives $Q_{s\min} = 383$ e⁻ at

$SNR_{output\min} = 1$;

– quantum efficiency of the PD $\eta_{PD} = 0.5$;

– time of charge accumulation on the PD $T_{acc} = 100$ μs;

– the number of cells of the PD per 2 resolution elements $n_{cell_s} = 18$.

The estimated value $DR_{HAOSA}^{(2)} = 66.73$ dB.

Given that $\eta_{Br}^{1W} = 0.5$ %, let us estimate the maximum input signal level $P_{sw_s\max} = 552$ mW. Here,

$DR_{HAOSA}^{(2)}$ includes a single-signal dynamic range

$DR_{HAOSA}^{(1)}$ with a common lower limit.

Let us take $SNR_{output\min} = 1$ and analyze expression (6) by squaring the expression:

$$Q_{s\min}^2 = \frac{Q_{max} + 2\sigma_q^2}{\pi} \left[2 + \sqrt{4 + 2\pi \left(2 - \frac{\pi}{2} \right)} \right]$$

At $Q_{max} \gg 2\sigma_q^2$, which is true for all cases presenting practical interest, $Q_{s\min}^2 \propto Q_{max}$. Then

$DR_{HAOSA}^{(2)}$ does not depend on Q_{max} , and is determined by the extent and duration of accumulation of the signal spectrum in the PD. It was previously mentioned that the necessary charge can be formed by both achieving the required level of the input signal and using the power of the laser and efficiently. In other words, by increasing P_{inc_s} , it is possible to lower the level of the input signal, while maintaining

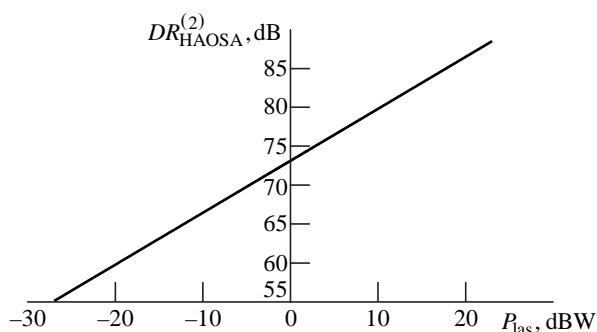


Fig. 5. Spurious Free Dynamic Range

the charge. In this case, a more linear character of the acousto-optical interaction corresponds to lower values of P_{inc_s} (see Fig. 4). Fig. 5 shows the dependence of $DR_{HAOSA}^{(2)}$ on the laser radiation power with a radiation utilization factor of 1%. The calculations were conducted using the previously defined parameters. The equality of $DR_{HAOSA}^{(2)}$ and $DR_{HAOSA}^{(1)}$ is achieved when the radiation power

$P_{las} = -19$ dB/mW for $Q_{max} = 10^5 e^-$, which can be provided by both a semiconductor [13, 14] and a gas laser [13, 15].

A longer accumulation period corresponds to a larger charge under the constant power at the AOM input, which also extends the two-signal dynamic range. Thus, the duration of accumulation can also be used to expand the two-signal dynamic range.

Conclusion. When substituting the parameters specified in [6], the developed statistical HAOSA model with a PD with accumulation provides a more accurate estimate of the dynamic range with an error of 1 dB compared to 4 dB obtained by the authors. The model also demonstrates the impossibility of a twofold increase (in decibels) in the dynamic range for interferometric circuits compared to power spectrum analyzers. This is determined by the necessity to provide a relatively high level of reference illumination in the spectral plane, which significantly increases the HAOSA intrinsic noise level.

References

1. Olbrich M., Mittenzwei V., Siebertz O., Schmulling F., Schieder R. A 3 GHz Instantaneous Bandwidth Acousto-Optical Spectrometer with 1 MHz Resolution. Proc. of 18th Intern. Symp. on Space Terahertz Technology, 21–23 March 2007, Pasadena, California, pp. 231–235. Available at: <https://hobbydocbox.com/Radio/95227070-A-3-ghz-instantaneous-bandwidth-acousto-optical-spectrometer-with-1-mhz-resolution.html> (accessed 16.01.2020).
2. Siebertz O., Schieder R., Gal C., Olbrich M., Hartogh P. Acousto-Optical Spectrometers for THz Heterodyne Instruments. Proc. SPIE. 4857, 2003, vol. 56.
3. Vander Lugt A. Interferometric Spectrum Analyzer. App. Opt. 1981, vol. 20, iss. 16, pp. 2770–2779. doi: 10.1364/AO.20.002770
4. Wiley W. A., Gatenby P. V. Theoretical Study of the interferometric Bragg-cell Spectrum Analyzer. IEE Proc. J. Optoelectronics. 1986, vol. 133, iss. 1, pp. 47–59. doi: 10.1049/ip-j.1986.0007
5. Tinoco A. F. S., Perrella W. J., Alves F. D. P., Oliveira J. E. B. Computer aided Design of Bragg Cell Spectrum Analyzer. Proc. of the 2001 SBMO/IEEE MTT-S Intern. Microwave and Optoelectronics Conf. Belem, Brazil, Brazil, 6–10 Aug. 2001, vol. 1, pp. 13–16. doi: 10.1109/SBMOMO.2001.1008708
6. Grachev S. V., Rogov A. N., Ushakov V. N. Homodyne Acousto-Optic Spectrum Analyzer with Spatial and Temporal Integration. Radioengineering. 2003, vol. 4, pp. 23–28. (In Russ.)
7. Saleh B. E. A., Teich M. C. Fundamentals of Photonics. 2nd ed. Hoboken, N. J., Wiley Interscience, 2007, 1177 p.
8. *Akustoopticheskie protsessory spektral'nogo tipa* [Acousto-Optical Spectral-Type Processors]. Ed. by V. V. Proklov, V. N. Ushakov. Moscow, Radiotekhnika, 2012, 192 p. (In Russ.)
9. Aronov L. A., Ushakov V. N. Quadrature Components Forming Method for Homodyne Acousto-Optic Spectrum Analyzer. J. of the Russian Universities. Radioelectronics. 2019, vol. 22, no. 2, pp. 53–61. doi: 10.32603/1993-8985-2019-22-2-53-61
10. Vander Lugt A. Optical Signal Processing. New York, Wiley Interscience, 2005, 604 p.
11. CCD Area Image Sensor S12101. Hamamatsu photonics. Available at: https://www.hamamatsu.com/resources/pdf/ssd/s12101_kmpd1176e.pdf (accessed 14.01.2020).
12. CCD Area Image Sensor S12101. Hamamatsu photonics. Available at: https://www.hamamatsu.com/resources/pdf/ssd/s12071_kmpd1138e.pdf (accessed 14.01.2020).
13. Svelto O. Principles of Lasers. 5th ed. New York, Springer Science+Business Media, LLC, 2010, 620 p.
14. Diode Lasers for Raman Spectroscopy. Micro Laser Systems, Inc. Available at: http://www.microlaser.com/PDFs/DL_for_Raman-16.pdf (accessed 14.01.2020).
15. HNL Series Red HeNe Lasers. User Guide Rev. B. August 21, 2018. Thorlabs. Available at: <http://cdn.specpick.com/images/photonics/products/HNL150RB.pdf> (accessed 14.01.2020).

Information about the authors

Leonid A. Aronov, Master's Degree in Telecommunications (2006), Senior Lecturer of the Department of Theoretical Bases of Radioengineering of Saint Petersburg Electrotechnical University. The author of 21 scientific publications. Area of expertise: optical information processing.

Address: Saint Petersburg Electrotechnical University, 5 Professor Popov Str., St Petersburg 197376, Russia

E-mail: Aronov.tor@gmail.com

<https://orcid.org/0000-0003-2332-7826>

Yurii S. Dobrolenskiy, Cand. Sci. (Phys.-Math.) (2008), Senior Researcher of the Space Research Institute of the Russian Academy of Sciences. The author of 60 scientific publications. Area of expertise: acousto-optics; physical optics; radio physics; fluctuation physics; atmospheric physics; space engineering; physics of planets.

Address: Space Research Institute of the Russian Academy of Sciences, 84/32 Profsoyuznaya Str, Moscow 117997, Russia

E-mail: dobrolenskiy@iki.rssi.ru

<https://orcid.org/0000-0003-4960-2232>

Gennadii V. Kulak, Dr. Sci. (Phys.-Math.) (2003), Professor (2011), Member of New York Academy of Sciences (1996), Professor of the Department of Physics And Mathematics of Mozyr State Pedagogical University named after I. P. Shamyakin. The author of 210 scientific publications. Area of expertise: acousto-optics of gyrotropic single crystals and optical waveguides; optoacoustics of condensed matter.

Address: Mozyr State Pedagogical University named after I.P. Shamyakin, 28/1 Studencheskaya Str., Mozyr 247760, Republic of Belarus.

E-mail: g.kulak57@mail.ru

Список литературы

1. A 3 GHz Instantaneous Bandwidth Acousto-Optical Spectrometer with 1 MHz Resolution / M. Olbrich, V. Mitzenzwei, O. Siebertz, F. Schmulling, R. Schieder // Proc. of 18th Intern. Symp. on Space Terahertz Technology, Pasadena, California, 21–23 March 2007. P. 231–235. URL: <https://hobbydocbox.com/Radio/95227070-A-3-ghz-instantaneous-bandwidth-acousto-optical-spectrometer-with-1-mhz-resolution.html> (дата обращения 16.01.2020).
2. Acousto-Optical Spectrometers for THz Heterodyne Instruments / O. Siebertz, R. Schieder, C. Gal, M. Olbrich, P. Hartogh. Proc. SPIE. 4857. 2003. Vol. 56.
3. Vander Lugt A. Interferometric spectrum analyzer // App. Opt. 1981. Vol. 20, iss. 16. P. 2770–2779. doi: 10.1364/AO.20.002770
4. Wiley W. A., Gatenby P. V. Theoretical Study of the interferometric Bragg-cell Spectrum Analyzer // IEE Proc. J. Optoelectronics. 1986. Vol. 133, iss. 1. P. 47–59. doi: 10.1049/ip-j.1986.0007
5. Tinoco A. F. S., Perrella W. J., Alves F. D. P., Oliveira J. E. B. Computer aided Design of Bragg Cell Spectrum Analyzer // Proc. of the 2001 SBMO/IEEE MTT-S Intern. Microwave and Optoelectronics Conf. Belem, Brazil, 6–10 Aug. 2001. Vol. 1. P. 13–16. doi: 10.1109/SBMO.2001.1008708
6. Грачев С. В., Рогов А. Н., Ушаков В. Н. Гомодинный акустооптический анализатор спектра с пространственным и временным интегрированием // Радиотехника. 2003. Вып. 4. С. 23–28.
7. Saleh B. E. A., Teich M. C. Fundamentals of Photonics. 2nd ed. Hoboken, NJ: Wiley Interscience, 2007. 1177 p.
8. Акустооптические процессоры спектрального типа / под ред. В. В. Проклова, В. Н. Ушакова. М.: Радиотехника, 2012. 192 с.
9. Аронов Л. А., Ушаков В. Н. Метод формирования квадратурных компонентов спектра в гомодинном акустооптическом спектроанализаторе // Изв. вузов России. Радиоэлектроника. 2019. Т. 22, № 2. С. 53–61. doi: 10.32603/1993-8985-2019-22-2-53-61
10. Vander Lugt A. Optical Signal Processing. New York: Wiley Interscience, 2005. 604 p.
11. CCD Area Image Sensor S12101 / Hamamatsu photonics. URL: https://www.hamamatsu.com/resources/pdf/ssd/s12101_kmpd1176e.pdf (дата обращения 14.01.2020).
12. CCD Area Image Sensor S12101 / Hamamatsu photonics. URL: https://www.hamamatsu.com/resources/pdf/ssd/s12071_kmpd1138e.pdf (дата обращения 14.01.2020).
13. Svelto O. Principles of Lasers. 5th ed. New York: Springer Science+Business Media, LLC, 2010. 620 p.
14. Diode Lasers for Raman Spectroscopy / Micro Laser Systems, Inc. URL: http://www.microlaser.com/PDFs/DL_for_Raman-16.pdf (дата обращения 14.01.2020).
15. HNL Series Red HeNe Lasers. User Guide Rev. B. August 21, 2018 / Thorlabs. URL: <http://cdn.specpick.com/images/photonics/products/HNL150RB.pdf> (дата обращения 14.01.2020).

Информация об авторах

Аронов Леонид Андреевич – магистр техники и технологии по направлению "Телекоммуникации" (2006), старший преподаватель кафедры теоретических основ радиотехники Санкт-Петербургского государственного электротехнического университета "ЛЭТИ" им. В. И. Ульянова (Ленина). Автор 20 научных работ. Сфера научных интересов – оптическая обработка информации.

Адрес: Санкт-Петербургский государственный электротехнический университет "ЛЭТИ" им. В. И. Ульянова (Ленина), ул. Профессора Попова, д. 5, Санкт-Петербург, 197376, Россия
E-mail: aronov.tor@gmail.com
<https://orcid.org/0000-0003-2332-7826>

Доброленский Юрий Сергеевич – кандидат физико-математических наук по специальности "Радиофизика" (2008), старший научный сотрудник Института космических исследований Российской академии наук (ИКИ РАН). Автор более 60 научных работ. Сфера научных интересов – акустооптика, физическая оптика, радиофизика, физика колебаний, физика атмосферы, космическое приборостроение, физика планет.

Адрес: Институт космических исследований Российской академии наук (ИКИ РАН), ул. Профсоюзная, д. 84/32, Москва, 117997, Россия
E-mail: dobrolenskiy@iki.rssi.ru
<https://orcid.org/0000-0003-4960-2232>

Кулак Геннадий Владимирович – доктор физико-математических наук (2003), профессор (2011), член Нью-Йоркской академии наук (1996), профессор кафедры физики и математики Мозырского государственного педагогического университета им. И. П. Шамякина, Республика Беларусь. Автор более 210 научных работ. Сфера научных интересов – акустооптика гиротропных монокристаллов и оптических волноводов; оптоакустика конденсированных сред.

Адрес: УО "Мозырский государственный педагогический университет им. И. П. Шамякина", ул. Студенческая, д. 28, Мозырь, 247777, Республика Беларусь
E-mail: g.kulak57@mail.ru
